

Spectral Modeling of SNe Ia Near Maximum Light: Probing the Characteristics of Hydro Models

E. Baron,^{1,2}

baron@nhn.ou.edu

Sebastien Bongard,^{1,3} David Branch,¹

branch@nhn.ou.edu

and Peter H. Hauschildt⁴

yeti@hs.uni-hamburg.de

ABSTRACT

We have performed detailed NLTE spectral synthesis modeling of 2 types of 1-D hydro models: the very highly parameterized deflagration model W7, and two delayed detonation models. We find that overall both models do about equally well at fitting well observed SNe Ia near to maximum light. However, the Si II 6150 feature of W7 is systematically too fast, whereas for the delayed detonation models it is also somewhat too fast, but significantly better than that of W7. We find that a parameterized mixed model does the best job of reproducing the Si II 6150 line near maximum light and we study the differences in the models that lead to better fits to normal SNe Ia. We discuss what is required of a hydro model to fit the spectra of observed SNe Ia near maximum light.

Subject headings: stars: atmospheres — supernovae: SN 1992A, SN 1994D, SN 1999ee

¹Homer L. Dodge Department of Physics and Astronomy, University of Oklahoma, 440 West Brooks, Rm. 100, Norman, OK 73019-2061, USA

²Computational Research Division, Lawrence Berkeley National Laboratory, MS 50F-1650, 1 Cyclotron Rd, Berkeley, CA 94720-8139 USA

³Institute de Physique Nucléaire Lyon, Bâtiment Paul Dirac Université Claude Bernard Lyon-1 Domaine scientifique de la Doua 4, rue Enrico Fermi 69622 Villeurbanne cedex, France

⁴Hamburger Sternwarte, Gojenbergsweg 112, 21029 Hamburg, Germany

1. Introduction

Intense astronomical interest has been focused on Type Ia supernovae since it was recognized long ago (Wilson 1939; Kowal 1968) that they are good “standard candles” and hence are useful cosmological probes. The reliability of SNe Ia as distance indicators improved significantly with the realization that the luminosity at peak was correlated with the width of the light curve (Phillips 1993) and hence that SNe Ia are correctable candles in much the same way that Cepheids are (Phillips et al. 1999; Goldhaber et al. 2001; Riess et al. 1995). With the discovery of the “dark energy” this interest has been further piqued (Riess et al. 1998; Garnavich et al. 1998; Perlmutter et al. 1999). Nevertheless, we still don’t know what the stellar progenitors for SNe Ia are, nor how they evolve with redshift. In addition, hydrodynamical modeling of SNe Ia explosions has now entered the sophisticated realm of fully 3-D hydro models (Röpke & Hillebrandt 2005; Gamezo et al. 2004, 2005). In spite of the sophistication of the modeling, the enormous dynamic range involved in modeling the fully turbulent flame propagation still requires the use of sub-grid models, or direct numerical simulation of small portions of the star (Zingale et al. 2005; Bell et al. 2004; Bell et al. 2004). In addition the 3-D models produce results that at first sight appear to be worse representations of the true phenomenon than the highly parameterized 1-D models. Deflagration models in particular appear to lead to ejecta configurations where unburnt C+O is mixed with burned material in such a way that the spectra produced by these models would differ significantly with observations. Kozma et al. (2005) showed that late-time spectra of a particular 3-D deflagration model would lead to strong [C I] and [O I] lines about 300 days after explosion that are unobserved in SNe Ia. The propensity for 3-D deflagration models to leave unburned C+O in the center has led to the suggestion that a detonation to deflagration transition (Gamezo et al. 2004, 2005) or a confined detonation (Plewa et al. 2004) is required to make the 3-D hydrodynamical models look more like the 1-D models which have stratified compositions.

Clearly the goal of SNe Ia explosion modeling is to perform full 3-D radiation hydrodynamics simulations with full reaction networks. Given present computer resources such realistic calculations are not yet feasible. Some parameterized 3-D synthetic spectral calculations have been performed (Kasen & Plewa 2005; Kasen et al. 2003b,a; Thomas et al. 2002), but calculations involving full detailed line and continuum NLTE still can only be performed in spherical symmetry.

2. Motivation

In previous work we have studied the detailed NLTE synthetic spectra of the parameterized 1-D model W7 (Nomoto et al. 1984; Thielemann et al. 1986) as well as the synthetic spectra produced by 1-D delayed detonation models (Höflich et al. 1998; Iwamoto et al. 1999) using the detailed generalized stellar atmosphere code PHOENIX (Lentz et al. 2001b,a; Nugent et al. 1997, 1995). Since that work, several improvements have been made to the PHOENIX code and more 1-D delayed detonation models have been calculated. In particular, more species have been added into NLTE in PHOENIX, and the treatment of the large dynamic range required to treat multiple ionization stages in NLTE has been improved through the use of up to 256-bit precision in solving the linear system for the rate equations, and in the EOS, making use of the QD package (Hida, Li, & Bailey 2001). Thus, up-to-date calculations should provide a better representation of the actual synthetic spectrum predicted by a particular hydrodynamical model. The hydrodynamic model we use is a somewhat modified version of the model presented in (Branch et al. 1985) in that we have extended the C+O layer from 22,000 km s⁻¹ to 30,000 km s⁻¹ using a density law $\rho \propto e^{-v/v_e}$ with $v_e = 2700$ km s⁻¹. The extension is necessary in order for the model to be optically thin in the UV and for it to reproduce the high velocity features that have been found in numerous SNe Ia (for example Hatano et al. 1999). This extension does not affect the total mass of the model.

Consequently, it makes sense to reexamine the synthetic spectra of both W7 and modern delayed detonation models. Here we focus on two particular delayed detonation models of Höflich et al. (2002) 5p0z22.25 which has $\Delta m_{15} = 1.00$ and 5p0z22.16 which has $\Delta m_{15} = 1.26$ (see Table 2 of Höflich et al. 2002).

Nugent et al. (1995) modeled a homogeneous model with a similar density structure to that of W7, and compositions obtained by mixing those of W7 above 8,000 km s⁻¹ using an older version of PHOENIX. They found that this model did a reasonably good job of reproducing the +5 day spectrum of SN 1992A and the maximum light spectrum of SN 1981B, but they treated only Ca II, Mg II, and Na I in NLTE.

Lentz et al. (2001a) used the fully stratified W7 hydro model and improved gamma-ray deposition to model a time series of spectra of SN 1994D. The species treated in NLTE were: H I, He I-II, C I, O I, Ne I, Na I, Mg II, Si II, S II, Ti II, Fe II, and Co II. They also used an earlier version of PHOENIX which did not handle the dynamic range associated with multiple ionization stages in NLTE in as sophisticated a manner as does the current version. In that work they were able to obtain acceptable fits to SN 1994D with W7, up until about March 18 (-3 days). After that epoch the quality of the fits deteriorated significantly, and prior to March 15, 1994, the Ca H+K feature was poorly fit by W7.

We have chosen to model the two supernovae that we had previously modeled, SN 1992A and SN 1994D, and the very well-observed SN 1999ee. All of these supernovae were well observed, SN 1992A has a *HST* UV+optical spectrum and thus offers wide wavelength coverage. The basic properties of these supernovae are listed in Table 1. While both SN 1992A and SN 1994D were moderately fast decliners, SN 1999ee was somewhat slower. The $B_{\max} - V_{\max}$ colors for all these supernovae is close to zero, but D. Branch et al. (in preparation) find that none of them is directly related to each other when the widths of the Si II λ 5972 and Si II λ 6355 lines are compared.

2.1. Methods

We have used the multi-purpose spectrum synthesis and model atmosphere code PHOENIX, version 13.11 (see Hauschildt & Baron 1999, 2004, and references therein). PHOENIX has been designed to accurately include the various effects of special relativity important in rapidly expanding atmospheres, like supernovae. Ionization by non-thermal electrons from γ -rays from the nuclear decay of ^{56}Ni that powers the light curves of SNe Ia is taken into account. We have used, an updated method for calculating the γ -ray deposition using a solution of the spherically symmetric radiative transfer equation for γ -rays with PHOENIX. We used an effective γ -ray opacity, $\kappa_{\gamma} = 0.06 Y_e \text{ cm}^2 \text{ gm}^{-1}$ (Colgate et al. 1980) for all calculations. The following species were treated in NLTE: H I, He I-II, C I-II, O I-III, Ne I, Na I-II, Mg I-III, Si I-III, S I-III, Ca II, Ti II, Fe I-III, and Co II. The atomic data used to construct the model atoms is taken from a variety of sources. The energy levels and radiative bound-bound cross sections are obtained from the work of Kurucz (Kurucz 1993, 1994a,b), the bound-free rates are based on data from the Opacity Project, the Iron Project, and other sources. The collisional rates are based on the Opacity project, Reilman & Manson (1979), and other sources.

The model structure for both W7 and the delayed-detonation models was taken from the output of the hydrodynamical models after they had reached the homologous phase. The abundances were also taken directly from the hydro models. The models were expanded homologously, and the decay of the radioactive species accounted for.

A rise time of 20 days after explosion to maximum light in B (e.g., Riess et al. 2000; Aldering et al. 2000) was assumed for all calculations. For W7, the hydrodynamic output was extended from $\sim 24000 \text{ km s}^{-1}$ to 30000 km s^{-1} with the unburned C+O white dwarf composition as in previous PHOENIX calculations using W7 (Nugent et al. 1997; Nugent 1997; Lentz et al. 2000, 2001a).

At each epoch, we have adjusted the total bolometric luminosity in the observer’s frame and we present results which provide the best fit (chi-by-eye) to match the shape and color of the observations. In each model the radiative transfer, the energy balance and NLTE rate equations are fully converged. About 150 models were constructed for the work reported here. Our methods involve the full solution to the NLTE radiative transfer problem including energy conservation. Gamma-ray deposition is treated as an explicit source term in the generalized equation of radiative equilibrium and no lightbulb is assumed.

In selecting the best fit, we first strive to fit the overall shape (or colors) and then we strive to fit the lineshape of selected lines. We are developing statistical tests to improve the sensitivity and we note that we are sensitive to much smaller variations of order 0.02 mag when this method is applied to SNe II (Mitchell et al. 2002, 2001; Baron et al. 2004).

3. Results

3.1. SN 1994D: Maximum Light

SN 1994D, in NGC 4526, was discovered 2 weeks before maximum brightness (Treffers et al. 1994). It was one of the best observed SNe Ia, with near-daily spectra starting 12 days before maximum brightness (-12 days) and continuing throughout the photospheric phase. SN 1994D has been well observed photometrically (Richmond et al. 1995; Patat et al. 1996; Meikle et al. 1996; Tsvetkov & Pavlyuk 1995) and spectroscopically (Filippenko 1997; Patat et al. 1996; Meikle et al. 1996). Wang et al. (1997) found no significant polarization in SN 1994D 10 days before maximum light. Cumming et al. (1996) placed a limit on a solar-composition progenitor wind of $1.5 \times 10^{-5} M_{\odot} \text{ yr}^{-1}$ for a 10 km s^{-1} wind. SN 1994D has been previously modeled with synthetic spectra and light curves by several groups (Hatano et al. 1999; Höflich 1995; Meikle et al. 1996; Mazzali & Lucy 1998; Branch et al. 2005).

Figure 1 displays our best fit for W7 compared to the spectrum of SN 1994D observed on March 21, 1994 (day -1). The observed spectra for SN 1994D have been dereddened by $E(B - V) = 0.06$ (cf. Drenkhahn & Richtler 1999), and de-redshifted using a recession velocity of 448 km s^{-1} . The fit is not bad and confirms that W7 is a reasonable first starting point for comparing hydrodynamic calculations to observations. The overall shape well reproduces the observed spectrum. The Ca II H+K line is nicely fit and the S II “W” is reasonably well fit. Nevertheless, the fit is poorest in the region around the defining feature of SNe Ia, Si II $\lambda 6355$. The Si II line is prominent and strong enough, but the absorption forms much too far out in the ejecta. The weaker Si II $\lambda 5972$ line is barely evident in the synthetic spectrum. This may be due to the extended blue wing of Si II $\lambda 6355$, which as we

discuss below is likely due to the interaction of Fe II/III line blending and the Si II line.

Branch et al. (2005) performed a detailed direct comparative analysis of the spectra of SN 1994D and even with a highly parameterized synthetic spectra code were not able to produce perfect fits at this epoch. When referring to features in the observed spectrum we will use the their line identifications.

In the work of Lentz et al. (2001a) the Si II $\lambda 5972$ line is prominent, although it is not strong enough in their model, it is still stronger than we find, this difference is almost certainly due to the more complete treatment of ionization stages in this work.

Figure 2 displays the synthetic spectrum of our best fit to SN 1994D at maximum light using the 5p0z22.16 model of Höflich et al. (2002). The bolometric luminosity is the same for both W7 and the delayed detonation model even though we searched for the best fit for both models varying this parameter. Although it is hard to quantify, the fit is about the same quality as that produced by W7. The Si II $\lambda 6355$ line is still too fast, as is the case for W7 the bluer Si II line is lost in the “red wing” of the redder Si II line. The S II “W” is reasonably well fit. The Fe III/Mg II/Si II feature just blueward of 4500 Å doesn’t match the continuum level, but the lineshapes are about right. Ca II H+K fits pretty well, but the Si II/Co II feature just to the red is not strong enough in the emission peak. Nevertheless, all of the features observed are reproduced in the synthetic spectrum.

Branch et al. (1985) calculated parameterized synthetic spectra of W7 and found that mixing the compositions above 10,000 km s⁻¹ improved the quality of the overall fit to SN 1981B. Harkness (1991) found that unmixed models actually were better when he included line blanketing in the UV. Nugent et al. (1995) found good fits to SN 1981B and SN 1992A with mixed W7 models. Full 3-D calculations (Röpke & Hillebrandt 2005; Gamezo et al. 2004; García-Senz & Bravo 2005) find that deflagrations lead inevitably to considerable mixing, so it is worth reconsidering the question of a mixed model here. In order to study mixing we replaced W7 with a parameterized model with a density determined by $\rho = \rho_0 e^{-v/v_e}$, where v_e is the e-folding velocity and ρ_0 is determined by setting the total continuum optical depth at 5000 Å, $\tau_{\text{std}} = 1$, at the “photospheric velocity”, v_0 , and the radius at that point $R_0 = v_0 t$, where t is the time since explosion. v_0 is determined by obtaining the best fit to the lineshapes. As always the total bolometric luminosity in the observer’s frame is an input parameter, here it is convenient to parameterize it in terms of the model temperature T_{model} . Except for the much more detailed NLTE treatment this is the identical procedure to that of Nugent et al. (1995). Figure 3 displays the result from the best fit to the parameterized mixed calculation 20 days after explosion. The mixed models assume gamma-ray deposition that follows the density profile. While the Si II $\lambda 6355$ line is well fit, the bluer $\lambda 5972$ line is just a bit too weak, the Si II “W” is well fit although the red

edge extends a bit too far to the red. The Si II/Co II feature just redward of 4000 Å is too weak and Ca II H+K is only reasonably well fit. Since we have altered the density structure, the compositions, and the gamma-ray deposition of W7, it would be incorrect to ascribe the improved fit of the Si II λ 6355 line simply to mixed compositions. We will discuss the line formation of Si II λ 6355 in detail in § 4

3.2. 1994D Postmax

Figure 4 displays the synthetic spectrum of our best fit to SN 1994D at maximum light using the 5p0z22.16/25 models of Höflich et al. (2002). Apart from the glaring absence of the strong observed Na D line the overall fit is not bad. Here the slower declining model 5p0z22.25 really appears to do a significantly better job at fitting the spectrum which likely is due to the fact that the post-maximum spectrum samples a larger amount of the ejecta, than do spectra at maximum light.

3.3. 1999ee

SN 1999ee is another extremely well observed SN Ia, with spectral coverage beginning 9 days prior to maximum light and continuing until 42 days after maximum. It was observed in the galaxy IC 5179 and was a relatively slow decliner with $\Delta m_{15} = 0.94$ (Hamuy et al. 2002). Krisciunas et al. (2004) quote an extinction of $A_V = 0.94 \pm 0.16$ for SN 1999ee or $E(B - V) = 0.3$.

Figure 5 compares the best fit synthetic spectrum for the W7 model to SN 1999ee on Oct 18, 1999 (Day -2). The overall quality of the fit is similar to that of SN 1994D, but with the additional wavelength coverage in the blue part of the observed spectrum, we see that the synthetic spectrum is too blue.

Figure 6 compares the best fit synthetic spectrum for the two delayed-detonation models to SN 1999ee on Oct 18, 1999. Since model 5p0z22.25 has a Δm_{15} closer to that of SN 1999ee (although it still declines a little too rapidly) should be a better fit to the observed spectrum. However, the fast decliner 5p0z22.16 fits much better (as was the case for SN 1994D, since the spectra at maximum are quite similar). This suggests that for spectra formation near maximum light the amount of nickel produced is not so important (if there is enough energy to reach the luminosity required). For the slow decliner 5p0z22.25, the lineshapes are overall not bad, but the continuum is too blue, particularly to the blue of Ca II H+K. However, the Si II λ 5972 line is stronger for the fast decliner, which is in the same sense as observed

empirically.

Figure 7 compares the best fit synthetic spectrum for the parameterized mixed model on day 20 to SN 1999ee on Oct 18, 1999 for two choices of T_{model} , 10,500 K and 11,500 K. The other parameters are the same as those for the 1994D uniform-composition model. The fit is not bad, the Ca II H+K is too slow, but the overall continuum shape is reasonably well reproduced, for the 10,500 K model.

It is possible that slow decliners have somewhat higher densities (which leads to higher opacities and thus longer risetimes). To test this we calculated a uniform model but at an earlier time. The velocity at the $\tau_{\text{std}} = 1$ was the same, but the e-folding velocity was smaller leading to a steeper density profile and hence higher density at $\tau_{\text{std}} = 1$. The result is shown in Figure 8. Although some of the lines are too narrow the fit is not bad, and the lines are forming at the right velocities. A model with an increased density can produce a reasonable fit. The narrowness of the lines in our synthetic spectrum is due to the choice of a steeper density profile, the lines could be made wider with a shallower density profile.

3.4. 1992A

The availability of an HST spectrum of SN 1992A provides a good opportunity to look at a broader wavelength range. Figure 9 compares the best fit synthetic spectrum for the two delayed-detonation models to SN 1992A on Jan 24, 1992 (HST) and Jan 25, 1992 (optical), roughly 5 days past maximum light. The fit is adequate, the overall shape of the spectrum is well reproduced, but most of the lines and continua do not fit well.

4. Discussion

As we have showed above, the optical spectra of W7 are similar in many respects to those of the delayed-detonation models, nevertheless the distribution of the energy over a wider wavelength region is significantly different. Figure 10 compares the day 20 spectra of W7, 5p0z22.16 and 5p0z22.25 where all models have the same bolometric magnitude. Clearly the W7 spectrum has a much smaller UV deficit than do the delayed-detonation models. This is illustrated in Table 2 where the absolute magnitudes in a wide range of photometric bands is listed. Clearly W7 is much bluer than the delayed detonation models even though we have kept M_{bol} fixed. All of the models are quite “blue” in $U - B$, but that is an intrinsic feature of SN 1994D.

Figure 11 compares the density profiles at day 20 of W7 to 5p0z22.16 and 5p0z22.25. The

Table 1. Parameters for Modeled SNe

SN	Δm_{15}	$B_{\max} - V_{\max}$
SN 1992A	1.47	0.02
SN 1994D	1.31	-0.05
SN 1999ee	0.94	-0.02

^aThe values for SN 1992A and SN 1994D were taken from Drenkhahn & Richtler (1999) and for SN 1999ee from Stritzinger et al. (2002).

Table 2.

Absolute Magnitude	W7	5p0z22.16	5p0z22.25
M_{bol}	-19.1	-19.1	-19.1
M_U	-20.10	-19.92	-19.82
M_B	-19.01	-19.29	-19.45
M_V	-18.72	-19.22	-19.32
M_R	-18.66	-19.22	-19.18
M_I	-18.26	-18.66	-18.44
M_Z	-18.27	-18.68	-18.54
M_J	-17.55	-18.21	-17.60
M_H	-17.41	-17.77	-17.51
M_K	-17.24	-16.79	-16.79

densities in the inner parts are nearly identical for all the models, W7 exhibits a characteristic “bump” where the deflagration dies out around $15,000 \text{ km s}^{-1}$, and the delayed detonation models have significantly higher densities than W7 in the outer parts.

Figure 12 compares the gamma-ray deposition function at day 20 of W7 to 5p0z22.16 and 5p0z22.25, except for the pronounced dip at the deflagration to detonation transition the shape of the deposition function is very similar to that of W7, particularly for model 5p0z22.25, which is about the same nickel mass as W7. In fact it is interesting to note that we obtained our best fit to SN 1994D at maximum light with model 5p0z22.16 which has only about $0.27 M_{\odot}$ of ^{56}Ni , not enough to produce the observed brightness of normal SNe Ia.

It is not easy to identify exactly why the Si II line absorption trough is too blue in W7 (and to a lesser extent in the delayed detonation models). It is tempting to point to the steep outer density gradient in W7 as the primary difference, however the uniform-composition models have an even steeper density gradient in the outer parts than does W7 and they in fact, fit the Si II feature best. The iron mass fraction is higher in the uniform models than in either W7 or in the delayed detonation models. Figs. 13 and 14 display the partial pressures of Si II–III and Fe II–III, respectively. The obvious difference between W7 and the other two models is that Fe III/Fe II and Si III/Si II strongly increases with velocity in W7, whereas it is nearly flat in both the delayed detonation model and in the uniform composition model. Stehle et al. (2005) found good fits to the Si II $\lambda 6355$ feature of SN 2002bo near maximum light, using the density profile of W7, but varying the compositions. They also found that they needed more iron in the outer parts of the atmosphere than W7 has. Interestingly, even with a large number of parameters, they weren’t able to well reproduce the sulfur “W” feature. Stehle et al. (2005) use a parameterized Schuster-Schwarzschild model and the Sobolev approximation and thus do not solve the full NLTE radiative transfer problem. However, they have fit the composition structure of by running a very large set of models (their code, with its simpler assumptions requires significantly less computer resources than do our models). Thus, given the fact that that they have altered the abundances in the model to get the best fit, they still do not reproduce the sulfur W, which leads us to suspect that it is the density structure (in a complicated combination with the abundances) that produces this feature and that is just what we have attempted to describe in this work.

Both the blue color of W7 and the fact that higher ionization stages increase with velocity leads us to conclude that W7 is “over-ionized”. This is not due to increased gamma-ray deposition as is clear from Fig. 12, but rather due to the steep density fall-off, or more correctly the steep fall-off of iron in the outer parts of W7. This steep fall-off in the iron abundance significantly reduces the UV deficit and thus there are more ionizing photons available to ionize the outer parts of the atmosphere.

It is clear (see for example Figure 7) that the blue part of the spectrum is extremely sensitive to the outer boundary condition (the total bolometric luminosity in the observer’s frame), thus the failure to fit the Si II and S II features seems to be generic to the models and not just an artifact of our choice of M_{bol} .

Branch et al. (2005) found that Si III was required in a velocity range from about 10,000–17,000 km s⁻¹ and that Si II was required from about 8,000–22,000 km s⁻¹. Figure 13 shows that all the models have significant Si II-III all the way out to the outermost layers of the atmosphere.

That Si II λ 6355 forms at high velocity in W7 even though the ratio of Si III/Si II is increasing is not surprising. The lower level is at 8.2eV, so some ionization actually will strengthen this line. Also, as we discuss in detail in a future publication (S. Bongard et al., in preparation) the actual line profile of the Si II λ 6355 and Si II λ 5972 lines is more likely due to complex radiative transfer effects involving Fe II and Fe III lines.

Quimby et al. (2006) studied the early spectra of SN 2005cg and concluded that the triangular shaped Si II λ 6355 feature was a unique prediction of the delayed-detonation models. However, Figure 1 clearly shows that W7 produces just such a line as late as maximum light. A direct confrontation of the spectra of W7 and the delayed-detonation models with the spectra of SN 2005cg will be the subject of future work.

5. Conclusions

Overall both the highly parameterized deflagration model W7 and the delayed detonation models that we have studied provide about equally good fits to spectra of normal SNe Ia near maximum light. The quality of the fit to near maximum light spectra is not strongly dependent on the distribution of nickel (or gamma-ray deposition) for the delayed detonation models (although we have forced the models to have the “right” luminosity, which is not self-consistent). W7 produces spectra that are both too blue, and where the Si II λ 6355 line (the defining feature of SNe Ia) is significantly too fast. This appears to be due to the rapid fall-off in the amount of iron in the outer layers of W7 and can be remedied either by flattening the density profile, or by increasing the relative fraction of iron. Our best fit model for the Si II λ 6355 feature near maximum had uniform compositions and a steeper overall density decrease than W7, which shows that the blue wing of the Si II feature found in W7 is due to material at high velocity and can be suppressed simply by removing that material. Clearly successful hydrodynamical models of SNe Ia require stratified compositions, nevertheless somewhat larger amounts of iron (whether it be primordial or produced in the

ejecta) seem to help. The delayed detonation models did a better job at reproducing the observed position of the Si II $\lambda 6355$ line and simply have a flatter density profile, so that may be an indication that flatter density profiles, as well as more iron in the outer layers is required.

We thank the anonymous referee for comments that improved the presentation. This work was supported in part by NASA grants NAG5-3505 and NAG5-12127, and NSF grants AST-0204771 and AST-0307323, PHH was supported in part by the Pôle Scientifique de Modélisation Numérique at ENS-Lyon. EB thanks the Laboratoire de Physique Nucléaire et de Haute Energies, CNRS-IN2P3, University of Paris VII, for a Professeur Invité when much of this work was done. This research used resources of: the San Diego Supercomputer Center (SDSC), supported by the NSF; the National Energy Research Scientific Computing Center (NERSC), which is supported by the Office of Science of the U.S. Department of Energy under Contract No. DE-AC03-76SF00098; and the Höchstleistungs Rechenzentrum Nord (HLRN). We thank all these institutions for a generous allocation of computer time.

REFERENCES

- Aldering, G., Knop, R., & Nugent, P. 2000, *AJ*, 119, 2110
- Baron, E., Nugent, P., Branch, D., & Hauschildt, P. 2004, *ApJ*, 616, 91
- Bell, J., Day, M., Rendleman, C., Woosley, S., & Zingale, M. 2004, *ApJ*, 608, 883
- Bell, J. B., Day, M. S., Rendleman, C. A., Woosley, S. E., & Zingale, M. 2004, *ApJ*, 606, 1029
- Branch, D., Baron, E., Hall, N., Melakayil, M., & Parrent, J. 2005, *PASP*, 117, 545
- Branch, D., Doggett, J. B., Nomoto, K., & Thielemann, F.-K. 1985, *ApJ*, 294, 619
- Colgate, S., Petschek, A., & Kriese, J. T. 1980, *ApJ*, 237, L81
- Cumming, R., Lundqvist, P., Smith, L., Pettini, M., & King, D. 1996, *MNRAS*, 283, 1355
- Drenkhahn, G. & Richtler, T. 1999, *A&A*, 349, 877
- Filippenko, A. V. 1997, in *Thermonuclear Supernovae*, ed. P. Ruiz-Lapuente, R. Canal, & J. Isern (Dordrecht: Kluwer), 1
- Gamezo, V., Khokhlov, A., & Oran, E. 2004, *Phys. Rev. Lett.*, 92, 211102

- . 2005, *ApJ*, 623, 337
- García-Senz, D. & Bravo, E. 2005, *A&A*, 430, 585
- Garnavich, P. M. et al. 1998, *ApJ*, 493, L53
- Goldhaber, G. et al. 2001, *ApJ*, 558, 359
- Hamuy, M. et al. 2002, *AJ*, 124, 417
- Harkness, R. 1991, in *Supernovae*, ed. S. E. Woosley (New York: Springer-Verlag), 454
- Hatano, K., Branch, D., Fisher, A., Baron, E., & Filippenko, A. V. 1999, *ApJ*, 525, 881
- Hauschildt, P. H. & Baron, E. 1999, *J. Comp. Applied Math.*, 109, 41
- . 2004, *Mitteilungen der Mathematischen Gesellschaft in Hamburg*, 24, 1
- Hida, Y., Li, X. S., & Bailey, D. H. 2001, in *15th IEEE Symposium on Computer Arithmetic*,
IEEE Computer Society, 155–162
- Höflich, P. 1995, *ApJ*, 443, 89
- Höflich, P., Gerardy, C., Fesen, R., & Sakai, S. 2002, *ApJ*, 568, 791
- Höflich, P., Wheeler, J. C., & Thielemann, F.-K. 1998, *ApJ*, 495, 617
- Iwamoto, K., Brachwitz, F., Nomoto, K., Kishimoto, N., Hix, W. R., & Thielemann, F.-K.
1999, *ApJS*, 125, 439
- Kasen, D., Nugent, P., Thomas, R. C., & Wang, L. 2003a, *ApJ*, 610, 876
- Kasen, D., Nugent, P., Wang, L., Howell, D. A., Wheeler, J. C., Höflich, P., Baade, D.,
Baron, E., & Hauschildt, P. 2003b, *ApJ*, 593, 788
- Kasen, D. & Plewa, T. 2005, *ApJ*, 21, L41
- Kowal, C. T. 1968, *AJ*, 73, 1021
- Kozma, C., Fransson, C., Hillebrandt, W., Travaglio, C., Sollerman, J., Reinecke, M., Röpke,
F., & Spyromilio, J. 2005, *A&A*, 437, 983
- Krisciunas, K. et al. 2004, *AJ*, 127, 1664
- Kurucz, R. 1993, *CDROM No. 1: Atomic Data for Opacity Calculations*, SAO Cambridge,
MA

- . 1994a, CDROM No. 22: Atomic Data for Fe and Ni, SAO Cambridge, MA
- . 1994b, CDROM No. 23: Atomic Data for Mn and Co, SAO Cambridge, MA
- Lentz, E., Baron, E., Branch, D., & Hauschildt, P. H. 2001a, *ApJ*, 557, 266
- . 2001b, *ApJ*, 547, 402
- Lentz, E., Baron, E., Branch, D., Hauschildt, P. H., & Nugent, P. 2000, *ApJ*, 530, 966
- Mazzali, P. A. & Lucy, L. B. 1998, *MNRAS*, 295, 428
- Meikle, W. P. S. et al. 1996, *MNRAS*, 281, 263
- Mitchell, R., Baron, E., Branch, D., Hauschildt, P. H., Nugent, P., Lundqvist, P., Blinnikov, S., & Pun, C. S. J. 2002, *ApJ*, 574, 293
- Mitchell, R., Baron, E., Branch, D., Lundqvist, P., Blinnikov, S., Hauschildt, P. H., & Pun, C. S. J. 2001, *ApJ*, 556, 979
- Nomoto, K., Thielemann, F.-K., & Yokoi, K. 1984, *ApJ*, 286, 644
- Nugent, P., Baron, E., Branch, D., Fisher, A., & Hauschildt, P. 1997, *ApJ*, 485, 812
- Nugent, P., Baron, E., Hauschildt, P., & Branch, D. 1995, *ApJ*, 441, L33
- Nugent, P. E. 1997, PhD thesis, University of Oklahoma
- Patat, F. et al. 1996, *MNRAS*, 278, 111
- Perlmutter, S. et al. 1999, *ApJ*, 517, 565
- Phillips, M. M. 1993, *ApJ*, 413, L105
- Phillips, M. M., Lira, P., Suntzeff, N. B., Schommer, R. A., Hamuy, M., & Maza, J. 1999, *AJ*, 118, 1766
- Plewa, T., Calder, A. C., & Lamb, D. Q. 2004, *ApJ*, 612, L37
- Quimby, R., Höflich, P., Kannappan, S., Rykoff, E., Rujopakarn, W., Akerlof, C., Gerardy, C., & Wheeler, J. C. 2006, *ApJ*, 636, 400
- Reilman, R. F. & Manson, S. T. 1979, *ApJS*, 40, 815
- Richmond, M. W. et al. 1995, *AJ*, 109, 2121

- Riess, A. et al. 1998, *AJ*, 116, 1009
- . 2000, *AJ*, 118, 2675
- Riess, A. G., Press, W. H., & Kirshner, R. P. 1995, *ApJ*, 438, L17
- Röpke, F. K. & Hillebrandt, W. 2005, *A&A*, in press, astro-ph/0411667
- Stehle, M., Mazzali, P., Benetti, S., & Hillebrandt, W. 2005, *MNRAS*, 360, 1231
- Stritzinger, M. et al. 2002, *AJ*, 124, 2100
- Thielemann, F.-K., Nomoto, K., & Yokoi, K. 1986, *A&A*, 158, 17
- Thomas, R., Kasen, D., Branch, D., & Baron, E. 2002, *ApJ*, 567, 1037
- Treffers, R. R., Filippenko, A. V., & Van Dyk, S. D. 1994, *IAU Circ.*, 5946
- Tsvetkov, D. Y. & Pavlyuk, N. N. 1995, *Astronomy Letters*, 21, 606
- Wang, L., Wheeler, J. C., & Höflich, P. 1997, *ApJ*, 476, L27
- Wilson, O. C. 1939, *ApJ*, 90, 634
- Zingale, M., Woosley, S. E., Rendleman, C., Day, M., & Bell, J. 2005, *ApJ*, 632, 1021

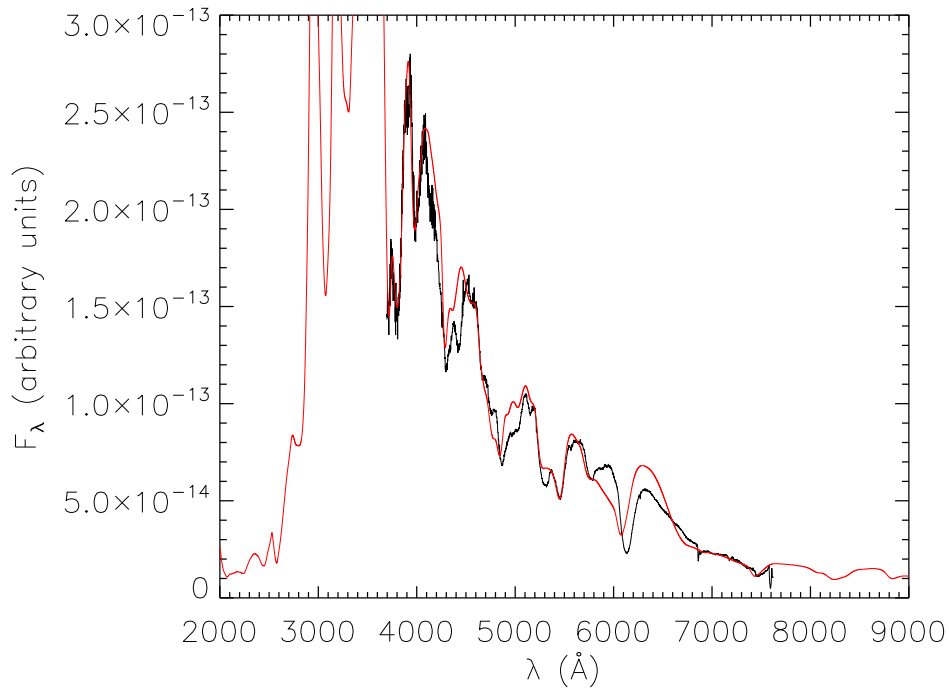


Fig. 1.— The synthetic spectra of a full NLTE model of W7, 20 days after explosion, is compared to the observed spectrum of SN 1994D on March 21, 1994 (the time of B maximum). In this and subsequent figures on SN 1994D the observed spectra have been corrected for redshift assuming a velocity of 448 km s^{-1} and a reddening of $E(B - V) = 0.06$.

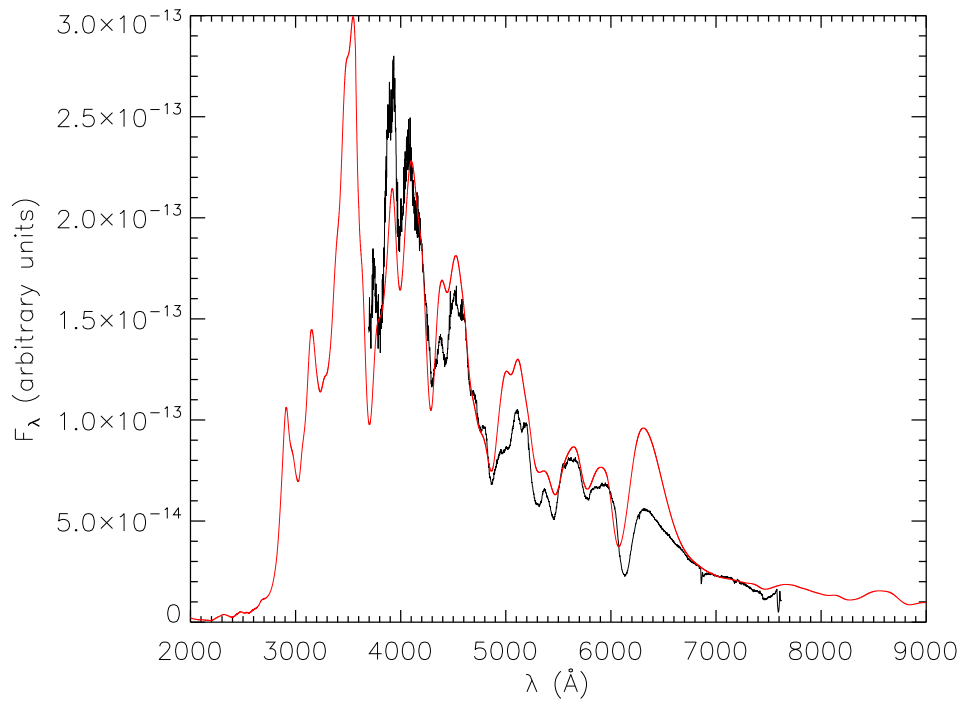


Fig. 2.— The synthetic spectra of a full NLTE model of hydro model 5p0z822_16 (red line), 20 days after explosion, is compared to the observed spectrum of SN 1994D on March 21, 1994 (the time of B maximum).

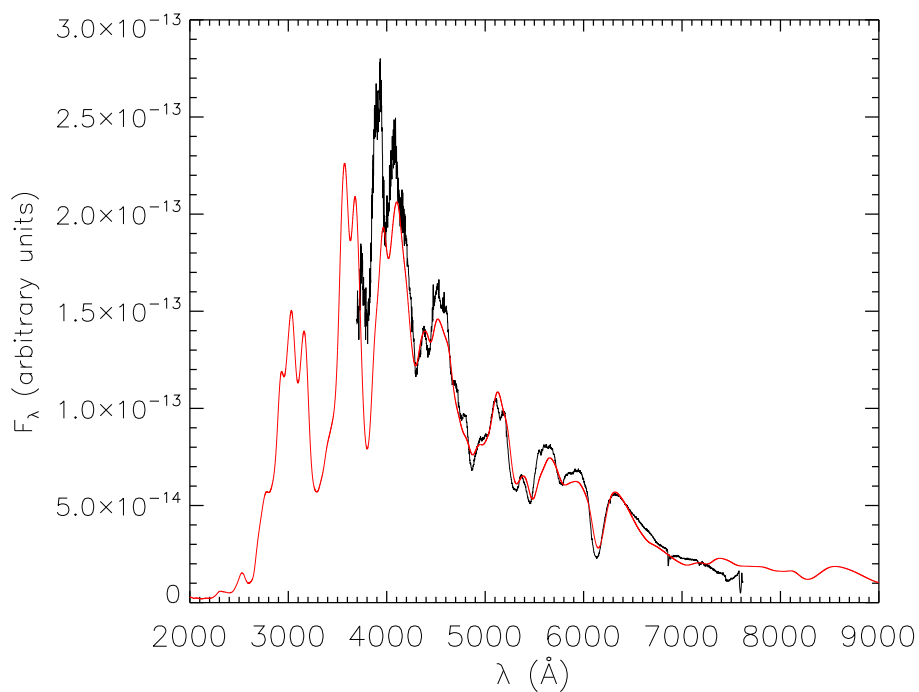


Fig. 3.— The observed spectrum of SN 1994D on March 21, 1994 (the time of B maximum) is compared to a synthetic spectra of a full NLTE parameterized model 20 days after explosion, where the compositions from W7 been artificially mixed to be uniform above the velocity point of 8000 km s^{-1} , the density profile has taken to be given by an exponential in velocity with $v_e = 1500 \text{ km s}^{-1}$, and the velocity at $\tau_{\text{std}} = 1$ is $7,500 \text{ km s}^{-1}$. The gamma-ray deposition follows the density profile.

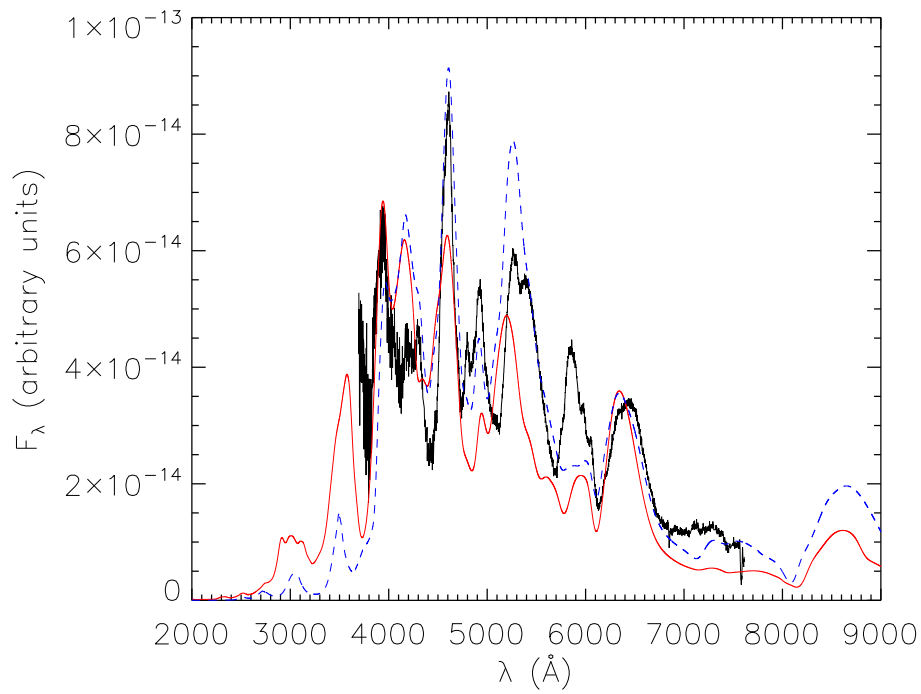


Fig. 4.— The synthetic spectra of a full NLTE models 5p0z822_16 (red line) and 5p0z822_25 (blue line), 35 days after explosion, are compared to the observed spectrum of SN 1994D obtained on Apr 5, 1994 (roughly 15 days after the time of B maximum).

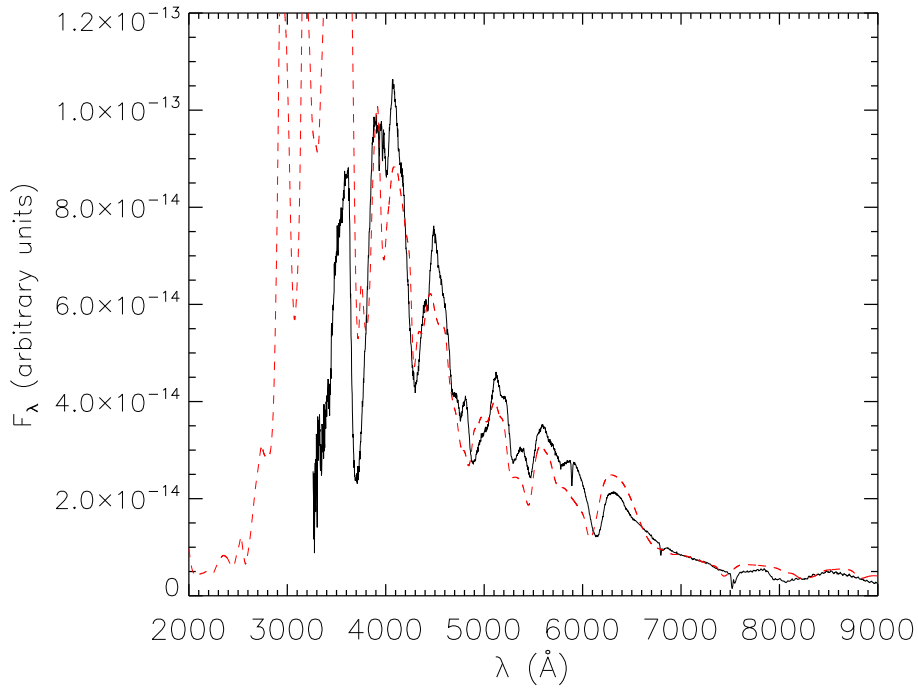


Fig. 5.— The synthetic spectra of a full NLTE model of W7, 20 days after explosion, is compared to the observed spectrum of SN 1999ee on October 18, 1999 (the time of B maximum). In this and subsequent figures on SN 1999ee the observed spectra have been corrected for redshift assuming a velocity of 3498 km s^{-1} (Hamuy et al. 2002) and a reddening of $E(B - V) = 0.30$ (Krisciunas et al. 2004; Stritzinger et al. 2002)

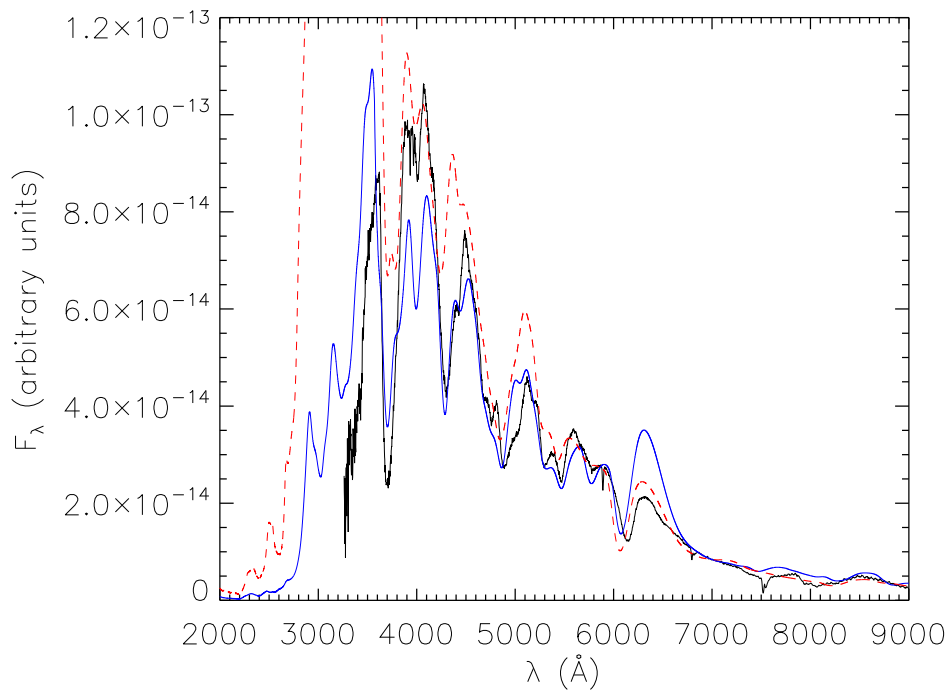


Fig. 6.— The synthetic spectra of a full NLTE models 5p0z822_25 (blue line) and 5p0z822_16 (red line), 20 days after explosion, are compared to the observed spectrum of SN 1999ee on October 18, 1999 (the time of B maximum).

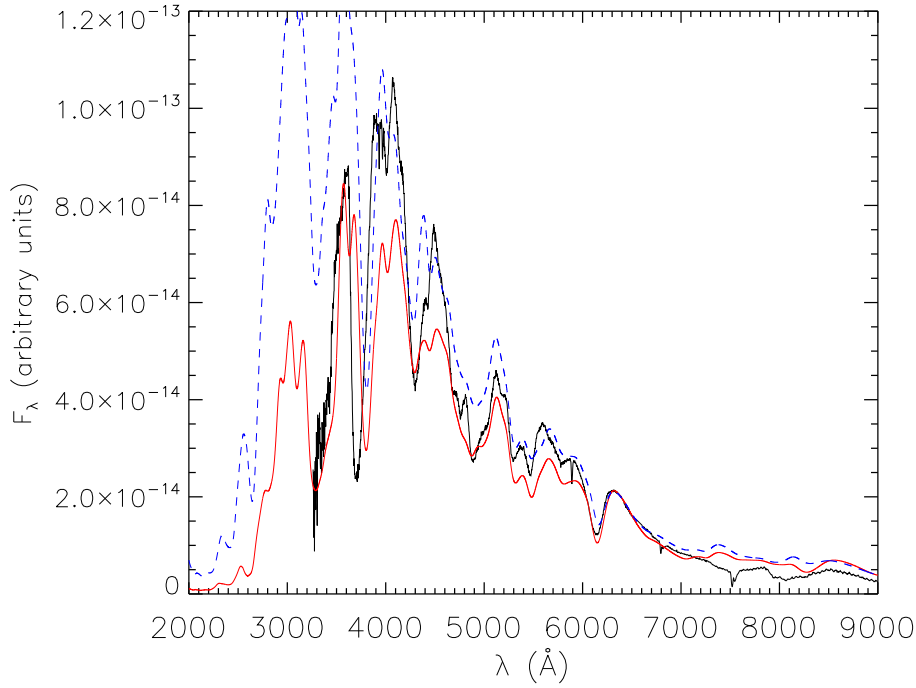


Fig. 7.— The observed spectrum of SN 1999ee on October 18, 1999 (the time of B maximum) compared with a synthetic spectra of a full NLTE model 20 days after explosion, where the W7 compositions have been artificially mixed to be uniform above the velocity point of 8000 km s^{-1} , the density profile has taken to be given by an exponential in velocity with $v_e = 1500 \text{ km s}^{-1}$, and the velocity at $\tau_{\text{std}} = 1$ is $7,500 \text{ km s}^{-1}$. The gamma-ray deposition follows the density profile. The red line has $T_{\text{model}} = 10,500 \text{ K}$ and the blue line $T_{\text{model}} = 11,500 \text{ K}$

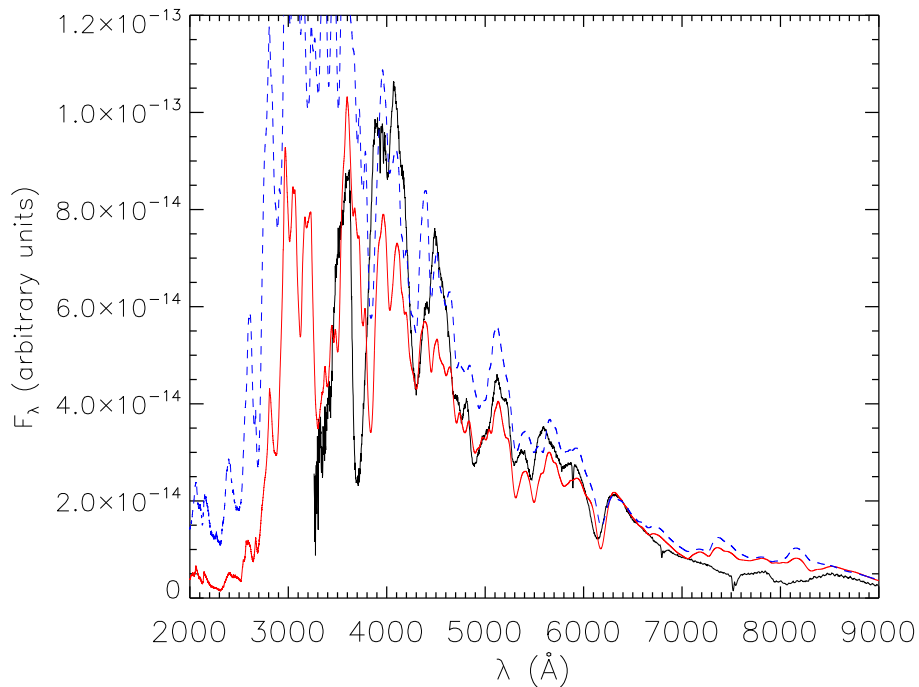


Fig. 8.— The observed spectrum of SN 1999ee on October 18, 1999 (the time of B maximum) compared with a synthetic spectra of a full NLTE model 15 days after explosion, where the W7 compositions have been artificially mixed to be uniform above the velocity point of 8000 km s^{-1} , the density profile has taken to be given by an exponential in velocity with $v_e = 900 \text{ km s}^{-1}$. There is no gamma-ray deposition. The red line has $T_{\text{model}} = 11,000 \text{ K}$ and the blue line $T_{\text{model}} = 12,000 \text{ K}$

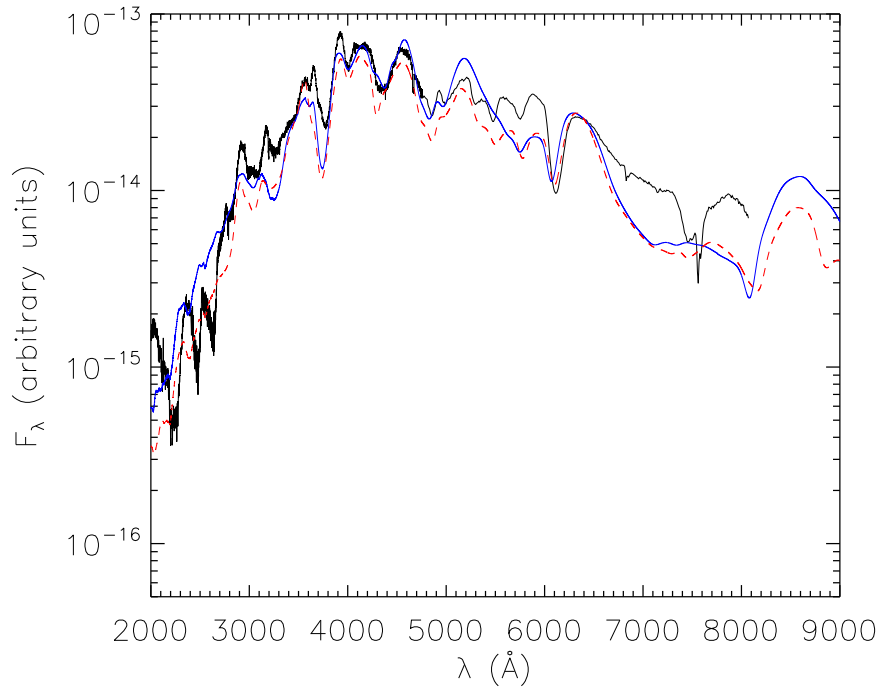


Fig. 9.— The synthetic spectra of a full NLTE models 5p0z822_25 (blue line) and 5p0z822_16 (red line), 25 days after explosion, are compared to the observed spectrum of SN 1992A obtained on Jan 25, 1992 (optical) and Jan 24, 1992 (HST) (roughly 5 days after the time of B maximum). The observed spectra have been corrected for redshift assuming a velocity of 1845 km s^{-1} and no reddening correction has been applied.

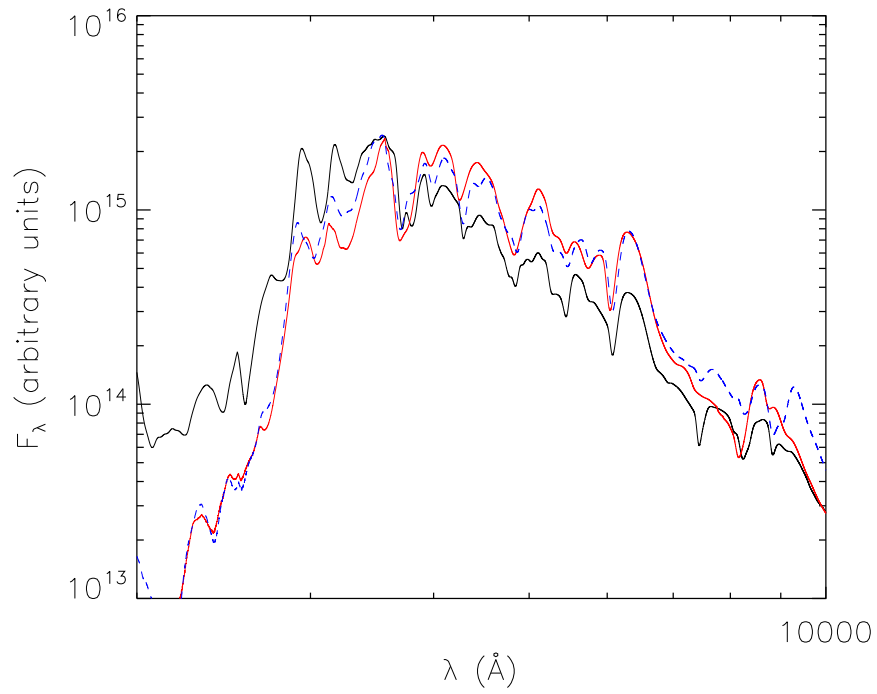


Fig. 10.— The synthetic spectra of a full NLTE models of W7 (black line), 5p0z822_16 (red line) and 5p0z822_25 (blue line), 20 days after explosion, are compared to each other.

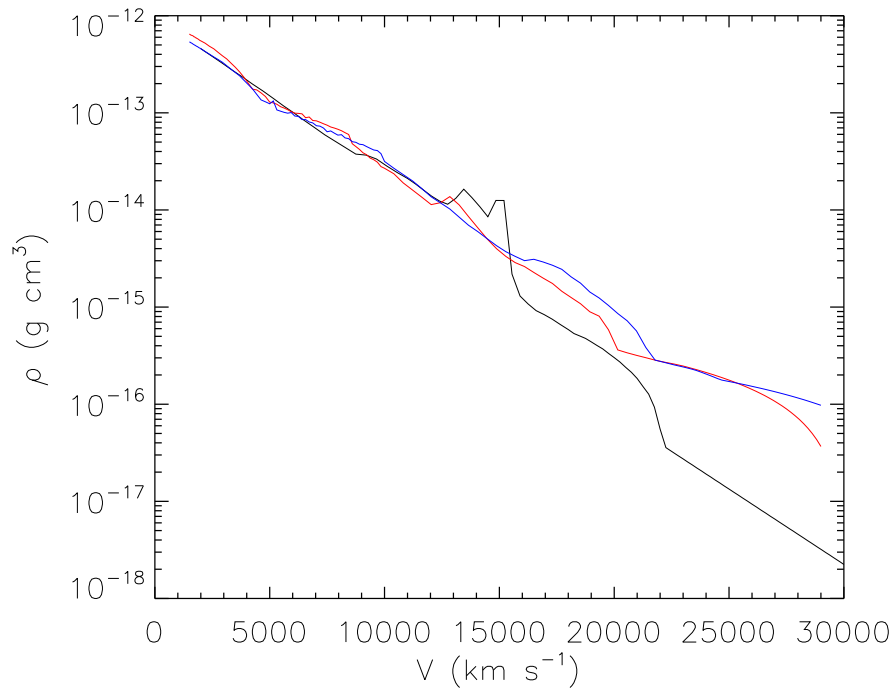


Fig. 11.— The density structure of W7 (black line), 5p0z822_16 (red line), and 5p0z822_25 (blue line), 20 days after explosion, are compared to each other.

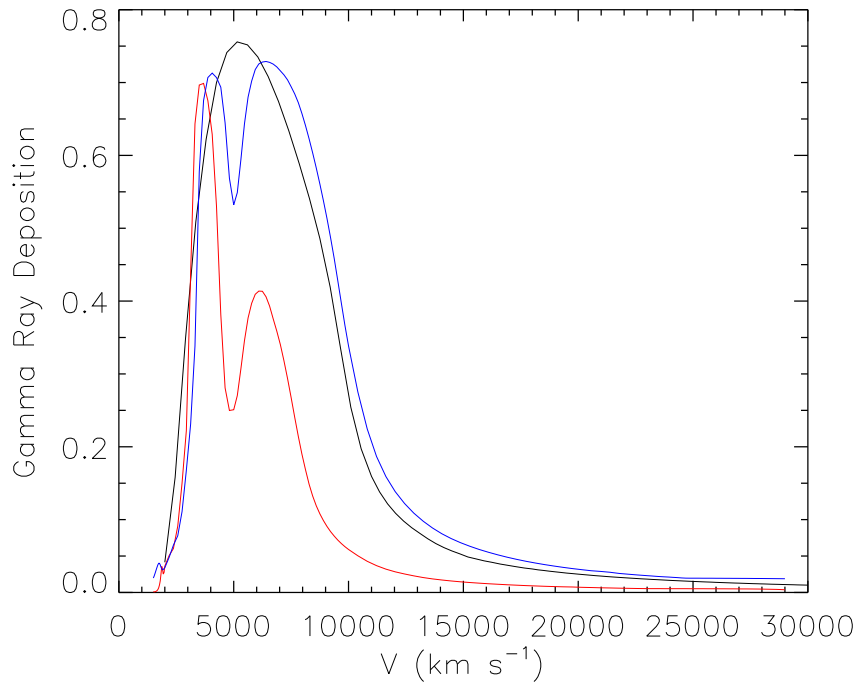


Fig. 12.— The gamma-ray deposition of W7 (black line), 5p0z822_16 (red line), and 5p0z822_25 (blue line), 20 days after explosion, are compared to each other.

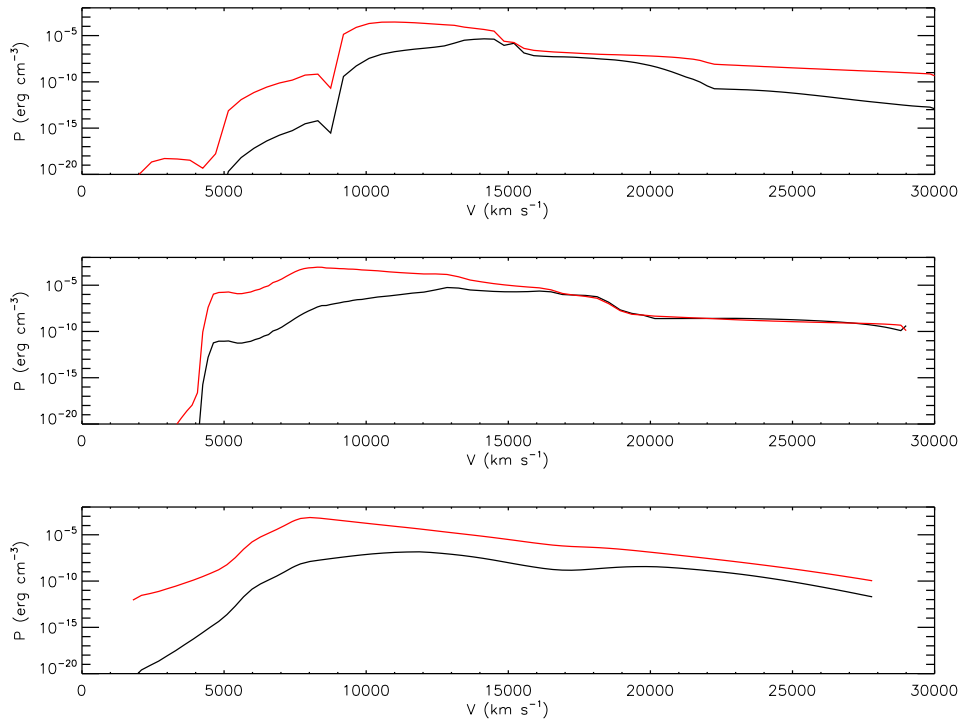


Fig. 13.— The partial pressures of Si II (black line) and Si III (red line) for W7 (top panel), the delayed detonation model 5p0z822_16 (middle panel), and the mixed model (bottom panel). Each model corresponds to the best fit for that particular model to SN 1994D.

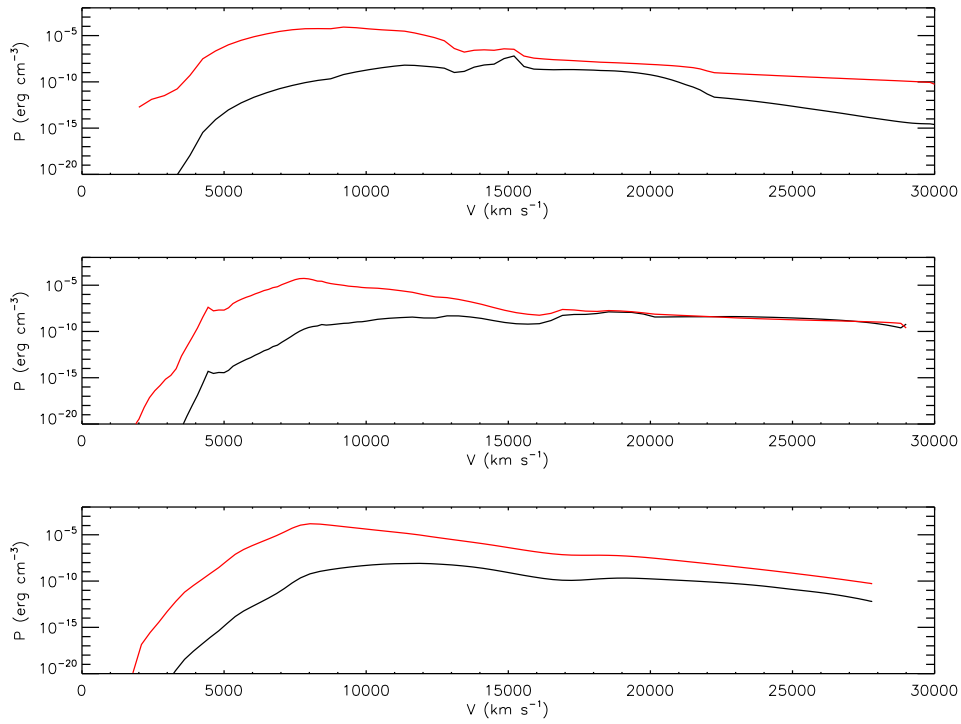


Fig. 14.— The partial pressures of Fe II (black line) and Fe III (red line) for W7 (top panel), the delayed detonation model 5p0z822_16 (middle panel), and the mixed model (bottom panel). Each model corresponds to the best fit for that particular model to SN 1994D.